

The Role of Magnetic Fields in the Interstellar Medium of the Milky Way

Evidence from the Diffuse Polarized Radio Emission

T.L. Landecker

Received: 5 November 2010 / Accepted: 7 June 2011 / Published online: 2 July 2011
© Springer Science+Business Media B.V. 2011

Abstract Synchrotron radiation is generated throughout the Milky Way. It fills the sky, and carries with it the imprint of the magnetic field at the point of origin and along the propagation path. Observations of the diffuse polarized radio emission should be able to provide information on Galactic magnetic fields with detail matching the angular resolution of the telescope. I review what has been learned from existing data, but the full potential cannot be realized from current observations because they do not adequately sample the frequency structure of the polarized emission, or they lack information on large-scale structure. I discuss three surveys, each overcoming one of these limitations, and show how use of complementary data on other ISM tracers can help elucidate the role of magnetic fields in interstellar processes. The focus of this review is on the small-scale field, on sizes comparable with the various forms of interaction of stars with their surroundings. The future is bright for this field of research as new telescopes are being built, designed for the survey mode of observation, equipped for wideband, multichannel polarization observations.

Keywords Galactic radio emission · Polarization · Magnetic fields · Faraday rotation · Rotation measure synthesis · Interstellar medium

1 Introduction

Magnetic fields pervade the interstellar medium (ISM) of the Milky Way. They are a significant reservoir of energy and play crucial roles in many interstellar processes because they are locked into the ISM plasma and add significantly to its pressure. Magnetic fields control the star-formation process, are essential to particle acceleration, and play a central role in the return of matter from stars to the ISM. Nevertheless, we still know very little about the details of these and other interactions of magnetic field with the ISM. It is usual to make a division between the large-scale field, on scales of the spiral arms,

T.L. Landecker (✉)
Dominion Radio Astrophysical Observatory, National Research Council Canada, Penticton, BC,
Canada, V2A 6K3
e-mail: tom.landecker@nrc.gc.ca

and the small-scale (quasi-random) field, on scales of stellar and other activity within the arms. At the Solar radius the large-scale field in the spiral arms is $\sim 2 \mu\text{G}$ and the small-scale random component is $\sim 3 \mu\text{G}$ (Sun et al. 2008). That the random field is larger than the regular field immediately implies strong interaction of interstellar processes with the field. Here I will discuss mostly the small-scale field and will concentrate on the information that observations yield on the role of magnetic fields in interstellar processes. General reviews of the magnetic field in the Milky Way and other galaxies abound (Heiles 1995; Beck 2001, 2009) but there are few reviews of the subjects dealt with here. I will emphasize both what is known and what is unknown, indicating fruitful directions for research.

Of the tracers of the Galactic magnetic field, synchrotron radio emission appears to be one of the most promising: it is generated everywhere in the Galaxy and there is Faraday rotation along virtually every path through the Galaxy as the emission propagates through the magnetized plasma. The polarization state is quite easy to measure at wavelengths from 1 cm to 1 m, and magnetic-field information should be available from such data with the full angular resolution of the telescope and potentially from the entire Galactic volume. Other tools for probing the field are more limited. Measurements of starlight polarization can give information on fields as a function of distance to a limit of a few kpc (Fosalba et al. 2002), and infrared observations promise a longer reach (Clemens et al. 2011). The Faraday rotation of signals from pulsars and extragalactic sources has given much information on large-scale fields (Han et al. 1997; Brown and Taylor 2001; Brown et al. 2003, 2007; Han 2009; Brown 2011; Van Eck et al. 2011; Noutsos 2011, *this issue*), but the spatial sampling is very sparse with present-day telescopes. Pulsars have associated distance information, but the Faraday rotation of extragalactic sources indiscriminately sums the entire line of sight through the Galaxy. Zeeman splitting of emission lines probes molecular clouds very well. Zeeman observations of H I may ultimately prove to be the best tool for measuring magnetic fields in the general ISM, but to date they have been successful in only a few hundred directions (Heiles and Robishaw 2009).

However, observations of the diffuse Galactic polarized emission have not lived up to their promise. On the technical side, we have not sampled the sky adequately, in either the spatial or frequency domains (and we have only recently come to understand this). On the scientific side, we have needed complementary observations of other components of the ISM that have not been available. Despite these limitations, much has been achieved, and I review what has been learned. Three datasets break free from these limitations to some extent, and I present significant results from them. We are on the cusp of major advances in this field, and I comment on the progress that will come from surveys underway and planned with the next generation of radio telescopes.

2 The Data

The first detections of polarized emission from the Galaxy (Westerhout et al. 1962; Wielebinski et al. 1962) were followed by investigations of the polarized sky at various wavelengths. By 1976 the number of polarization observations of extensive areas had reached 18—listed by Spoelstra (1984). The most thorough were the surveys carried out with the Dwingeloo telescope at five frequencies from 408 to 1411 MHz. Observed between 1961 and 1966, and published by Brouw and Spoelstra (1976), these surveys have careful absolute calibration and correction for instrumental effects, and they appear to cover most of the northern sky. However, at 1411 MHz the 1726 pointings sample only $\sim 3\%$ of the sky accessible to the telescope. At the lowest frequency, 408 MHz, with a broader beam, this fraction rises to $\sim 20\%$.

Table 1 Surveys of the Galactic polarized emission

Survey	Ref.	ν [MHz]	θ [']	A-S	S-A	Large Scale	RM Synth.	Coverage [Sr]
WSRT-150	(1)	139–153	2	y		n	y	1×10^{-2}
WENSS	(2)	325	8	y	y	y?	n	0.3
WSRT-350	(3)	341–375	5			n	n	1.6×10^{-3}
WSRT-RMS	(4)	324–387	4			n	y	2.6×10^{-2}
Dwingeloo	(5)	408	138		y	y	n	7.0
		465	120		y	y	n	7.0
		610	90		y	y	n	7.0
		800	60		y	y	n	7.0
		1411	36		y	y	n	7.0
EMLS	(6)	1400	9.4		y	n	n	2.3
DRAO 26m	(7)	1410	36		y	y	n	9.1
Villa-Elisa	(8)	1420	36		y	y	n	5.2
CGPS	(9)	1420	1	y	y	y	n	0.37
SGPS	(10)	1336–1432	2	y		n	n	9.6×10^{-2}
Eff-11	(11, 12)	2695	5			n	n	0.21
Pks-11	(13)	2417	10		y	some	n	0.71
PGMS	(14)	2300	9		y	n	y	8.7×10^{-2}
Urumsqi	(15, 16)	4800/4963	10		y	y?	n	0.32
WMAP-23	(17)	23000	120			y	n	12.6

References: (1) Bernardi et al. (2009), (2) Schnitzeler et al. (2007), (3) Haverkorn et al. (2003), (4) Schnitzeler et al. (2009), (5) Brouw and Spoelstra (1976), (6) Reich et al. (2004), (7) Wolleben et al. (2006), (8) Testori et al. (2008), (9) Landecker et al. (2010), (10) Haverkorn et al. (2006), (11) Junkes et al. (1987), (12) Duncan et al. (1999), (13) Duncan et al. (1997), (14) Carretti et al. (2010), (15) Sun et al. (2007), (16) Gao et al. (2010), (17) Hinshaw et al. (2009)

Notes: (a) ν , frequency in MHz. (b) θ , beamwidth in arcminutes. (c) A-S denotes aperture synthesis, S-A denotes single antenna. (d) y or n under the heading “Large Scale” indicates that large-scale structure is or is not represented. y? indicates that large-scale structure has been incorporated incompletely and/or derived from observations at another frequency—see discussion in Sect. 3.2. (e) y under RM Synth. indicates that the data are adequate for application of RM Synthesis. (f) Coverage gives the sky area observed in steradians

In the 1980s polarization observations using large single-antenna radio telescopes began again, initiated with the Effelsberg 100-m Telescope, starting with the work of Junkes et al. (1987), this time with more thorough or even complete sampling, but usually concentrating on the Galactic plane. The most recent of this series, the Effelsberg Medium Latitude Survey (EMLS—Reich et al. 2004) extends coverage to $-20^\circ < b < 20^\circ$ at 1400 MHz. These have been joined by surveys using aperture-synthesis telescopes, achieving higher angular resolution. Table 1 lists surveys, and observations of lesser scope, that give valuable information on the polarization of the Galactic synchrotron emission. Note that the CGPS survey incorporates data from the EMLS and the DRAO 26 m survey with aperture-synthesis data: see Sect. 5.2 for more detail. The surveys of Table 1 represent a major observational effort, and we have learned much from them (reviewed in Sect. 4). Nevertheless, they have major shortcomings. In the next section I discuss what really needs to be measured in order to make advances in the astrophysics of the magneto-ionic medium (MIM).

3 Technical Requirements

The polarized sky does not resemble the total-intensity sky. The reason, understood from the beginning, is that Faraday rotation occurs along the propagation path between the source of the emission and the telescope. When polarization angle, θ [rad], is measured as a function of wavelength, λ [m],

$$\Delta\theta = \zeta\lambda^2 = 0.81\lambda^2 \int n_e B_{\parallel} dl \quad (1)$$

where ζ [rad m^{-2}] is the Faraday depth (Burn 1966), n_e [cm^{-3}] is the electron density, B_{\parallel} [μG] is the line-of-sight component of the magnetic field, and the integral extends along the entire line of sight. Under simple circumstances, a Faraday screen distinct from and in front of a background synchrotron emitter, $\zeta = \text{RM}$, the rotation measure.

If Faraday rotation is dominant in shaping the polarized sky, then we will not understand the ISM by simply measuring θ at one wavelength: *the physically significant quantity is Faraday depth (or rotation measure), the product of magnetic field strength and electron density*. Measuring this quantity immediately implies making polarization measurements at a number of frequencies. In Sect. 3.1 I discuss the sampling in the frequency domain that is required to probe polarization structure.

The Milky Way is all around us, and synchrotron emission is generated throughout. Galactic radio emission therefore has structure on all scales from large to small. If the large-scale structure is missing or under-represented in polarization measurements the polarization angle cannot be established; this is a major defect in many polarization datasets and limits their value for astrophysical interpretation. I discuss spatial sampling in Sect. 3.2.

3.1 Adequate Sampling in Frequency

Synchrotron radiation is broadband by nature. To determine the spectrum of total-intensity emission from the Milky Way or from a typical extragalactic source requires only a handful of measurements spanning the microwave spectrum: synchrotron emission can be characterized by a small number of parameters (as can mixed thermal and synchrotron emission). On the other hand, the Faraday rotation effects along the propagation path are usually not so simple. For example, Reich et al. (2004) and Gao et al. (2010) present data on a large area near the anticentre at 1.4 GHz and 4.8 GHz respectively, with very similar angular resolution ($\sim 10'$). The total-intensity images are unmistakably similar, but there is little resemblance in polarization structure at the two frequencies. Towards the inner Galaxy matters are worse. The probable cause is the interaction of a number of Faraday-rotation phenomena, such as beam depolarization and depth depolarization—differential Faraday rotation—(Burn 1966; Sokoloff et al. 1998). At the lower frequencies the ISM can become Faraday thick, and telescopes operating at widely separated frequencies may sample different volumes.

The question then arises: what sampling in frequency *is* required to characterize the extended polarized emission? We do not know the full answer yet, and probably will not until the Galactic plane has been extensively re-observed with adequate tools. Nevertheless, it is quite clear that we need polarimetric data measured in many adjacent channels across wide bands. The need for data of this kind, and methods for their analysis were laid out by Burn (1966), but technical limitations made acquisition and analysis of such data impossible until recently. Such methods are now easily implemented as Rotation Measure Synthesis (Brentjens and de Bruyn 2005; Heald 2009).

In (1) $\zeta = \text{RM}$ under very simple circumstances, where a source of polarized emission lies behind the Faraday rotating screen, and this is an adequate assumption when these conditions are approximately true (for example when studying a compact extragalactic source seen through the Galactic ISM). In the Galaxy, emission and Faraday rotation are thoroughly intermixed, and both occur virtually everywhere; under these conditions θ does not have a linear dependence on λ^2 . RM Synthesis may still be able to recover the polarization structure along the line of sight (not completely, but to a useful extent). Choosing a value for ζ , the observed polarization vector in each channel is rotated by $\zeta\lambda^2$ and the rotated vectors are coherently added to obtain an image of polarized intensity at that value of Faraday depth.

We do not know exactly how much resolution in Faraday depth is required, but we infer from existing data (Schnitzeler et al. 2009) that a value of $\sim 10 \text{ rad m}^{-2}$ is useful for regions off the Galactic plane. This implies observing down to frequencies of order 300 MHz: the resolution in Faraday depth depends on the longest wavelength observed—Brentjens and de Bruyn (2005), Schnitzeler et al. (2009). Such observations have their own complications, including ionospheric Faraday rotation and heavy RFI. Furthermore, turbulence in the MIM will produce dispersion in Faraday depth, leading to depolarization (Burn 1966) that is especially significant at long wavelengths since the effect depends on λ^4 . Observations near 300 MHz may have limited value at low Galactic latitudes. The GMIMS survey (Sect. 5.4) will extend down to 300 MHz, and analysis of these data will answer some of the questions asked here.

Nor do we know how thoroughly we need to sample λ^2 space. For example, it is conceivable that sampling a moderate number of narrow channels across a wide total bandwidth is adequate. The rotation measure spread function (Brentjens and de Bruyn 2005) will have bad sidelobes, but these can be removed (partly) by deconvolution, a CLEAN process (Heald 2009). This process interpolates in λ^2 space, filling in the missing frequency channels from information at other frequencies. Modelling may give useful guidance, but, at this stage, without experience in analyzing actual data, it is impossible to decide how risky this is. Given the complexity that we find in the ISM, it seems advisable to strive for the fullest frequency coverage possible: measured data is always better than reconstructed data. Existing analyses of MIM structures where emission and Faraday rotation are mixed are confined to those situations that can be treated analytically (Burn 1966; Sokoloff et al. 1998) and these are simple situations.

The absence of information at *short* wavelengths from RM Synthesis data imposes an upper limit to the largest Faraday-depth structure that can be detected. A Faraday slab, in which emission and rotation both occur, produces smooth, extended features in RM space. Such a feature will be “differentiated” and break up into delta functions where sharp transitions in RM occur at the front and back of the slab. This is analogous to the problem in interferometric imaging where the absence of data from short baselines hides large physical structure (Brentjens and de Bruyn 2005; Schnitzeler et al. 2009). A further limitation of RM Synthesis is its inability to recover the intrinsic polarization angle (the angle at $\lambda = 0$) because it is impossible to make measurements at negative values of λ^2 . Frick et al. (2010, 2011) discuss the use of symmetry arguments and wavelet-based RM Synthesis to help overcome this problem.

The product of RM Synthesis is a data cube of complex numbers, a set of images of polarized intensity and polarization angle at different values of Faraday depth. The sensitivity of each image is determined by the entire bandwidth of the observations, which is usually very large. As a consequence, the new generation of instruments is producing polarization images whose sensitivity far exceeds anything that existed hitherto. With this great sensitivity and with the ability to analyze the MIM in a new way, we are on the cusp of a new era in the study of the extended polarized emission from the Milky Way.

3.2 Sampling Structure on All Scales

Our understanding of other constituents of the ISM has been transformed by the attainment of angular resolution of order one arcminute in recent extensive surveys along the Galactic plane, the Canadian Galactic Plane Survey—the CGPS—(Taylor et al. 2003), and its companions, the Southern Galactic Plane Survey—the SGPS—(McClure-Griffiths et al. 2001), and the VLA Galactic Plane Survey—VGPS—(Stil et al. 2006). We can expect the same to be true of the magnetic field.

How much angular resolution is adequate for studying the polarized ISM? The glib answer is that the highest resolution is never enough, that there are always problems just beyond the reach of the telescope. As a guideline, one arcminute seems a reasonable target because this is the stellar separation in the nearest spiral arms. If we can understand arc-minute data we will be ready to take on the next challenge.

Such resolution at decimetre wavelengths demands use of aperture-synthesis (A-S) techniques. Since A-S telescopes are not sensitive to the largest structures, it is immediately apparent that single-antenna (S-A) data will have to be incorporated. A problem appears at once, because adequate S-A polarization data are not available. To date, only one polarization survey has met this challenge, the CGPS Polarization Survey (Landecker et al. 2010)—see Sect. 5.2. High quality wideband spectropolarimetric data obtained with S-A telescopes will be vital if progress is to be made in this field (see Sect. 5.4).

Why do many of the surveys made with S-A telescopes not include large-scale structure (Table 1) when such telescopes are inherently able to detect structure on all scales? When making polarization observations with S-A telescopes there is no point in the sky where the polarized signal is zero: there is always a contribution from instrumental polarization and from ground emission (not itself polarized, but converted to apparently polarized emission by the antenna sidelobes). Measuring ground emission and instrumental polarization on an absolute scale is difficult. This problem is avoided in the EMLS (Reich et al. 2004) (and most other S-A polarization surveys) by observing the sky one small patch at a time. Over that small patch ground emission will be approximately constant and instrumental polarization will be stable over the short time of the observation. Subtracting the mean value of Q and U from the observations then removes these effects, but it also filters off large structure. The extent of this filtering depends on the size of the patches that make up the observations. In the case of the EMLS this is typically $10^\circ \times 10^\circ$, and polarized structures of $\sim 5^\circ$ and larger are seriously under-represented. This feature of the EMLS is fully discussed by Reich et al. (2004)—see Fig. 3 of that paper—and emphasized again by Reich (2006). The extent to which large structure is filtered off when scanning with a S-A telescope depends critically on the extent of the scans that make up the data: the very best result is obtained by observing the entire sky (see, for example, Carretti 2011).

The ISM is turbulent, and electron density, field direction and field strength have spatial variability. As a result Faraday rotation can break large, smooth total-intensity structures into smaller polarization features. If this effect is sufficiently strong there will be virtually no large structure in polarization images. Is it then necessary to add S-A data to A-S data? Available evidence suggests that it is. Large-scale structure is definitely present in the CGPS polarization survey at 1420 MHz (see Fig. 8 of Landecker et al. 2010). From S-A radio telescope data we see that significant polarized emission remains in a 2° beam at 408 MHz (Brouw and Spoelstra 1976) and in a 1.5° beam at 240 MHz (Wilkinson 1973). However, it is hard to generalize about this question.

Despite everything that I have said here, datasets that miss broad structure are still valuable for the *identification* of interesting polarization structures—e.g. Rudnick and Brown (2009).

4 What Have We Learned?

The observations listed in Table 1 may have their limitations, but we have learned much from their data. In this section I discuss some of the conclusions reached from observations of the diffuse polarized emission from the Milky Way.

4.1 Sensitivity of Polarization Observations to Ionized Gas

A typical radio telescope operating at decimetre wavelengths is more sensitive to the Faraday rotation in a volume of ISM plasma than to its bremsstrahlung. Consider an ionized region of extent 10 pc with electron density 0.5 cm^{-3} in a magnetic field with a line-of-sight component of $2 \mu\text{G}$ (typical ISM conditions). At 1.4 GHz this region produces a Faraday rotation of 20° , which is easy to detect. The same region produces an emission measure of $2.5 \text{ cm}^{-6} \text{ pc}$, a challenge for the most sensitive radio telescope to detect in total intensity. This is the origin of the frequent comment that the polarized sky does not resemble the total-intensity sky. However, the sensitivity of H α surveys is superior. The Wisconsin H α Mapper—WHAM—(Haffner et al. 2003) can reach levels of emission measure ten times lower than most radio telescopes, and the polarized sky often bears a stronger resemblance, either correlation or anti-correlation, to the H α sky (limited, of course, by optical extinction). A detailed study of these resemblances covering a large area has not yet been made.

4.2 The Distance to Polarization Features

As in any astronomical endeavor, determining distance is important in assessing the physical properties of a polarization feature. Physical size is significant, for example, in establishing scale sizes of turbulence. The path length through a Faraday rotating structure must be known if a magnetic field estimate is to be derived from a Faraday depth measurement (and, of course, independent data on electron density are also needed).

H I absorption is a powerful technique for determining (or limiting) distance to continuum emitters. This can be applied to polarized emission, but not without difficulty. On the positive side, H I emission is unpolarized, so confusion from small emission regions in the off-source area is not a problem (this is the limiting factor in total-intensity absorption work). On the negative side, signal-to-noise ratios are very low. Dickey (1997) has applied this technique to determine the distance to the extended Galactic polarized emission in a small target area at $\ell = 329.5^\circ$, $b = 5^\circ$: the derived distance was 2 kpc. The only further application of this difficult technique has been its use by Kothes et al. (2004) to determine H I absorption distances to supernova remnants of low surface brightness.

Depolarization by H II regions can be used as an aid in distance determination. If the outline of the H II region corresponds with an area of reduced polarized intensity, the association is usually firm, and the polarization feature definitely lies behind the H II region (whose distance is often independently known). There are several caveats. First, some H II regions have quite regular fields, and will not necessarily depolarize (see Sect. 4.4). Second, the depolarization due to an H II region will not necessarily be total: the ISM on the near side of the H II region can be a synchrotron emitter, and itself a polarized emitter. In the CGPS survey (Landecker et al. 2010, Sect. 5.2) there are many instances in which Local-arm H II regions depolarize more distant Perseus-arm features. The foreground emission is relatively smooth, and the emission coming from larger distances shows structure on smaller angular scales; an unambiguous distance limit can then be deduced.

Two effects combine to determine a “polarization horizon”: polarized signals originating beyond the polarization horizon cannot be received (Uyaniker et al. 2003). First, the ISM

is Faraday thick and signals from further away are depolarized. Second, the telescope beam embraces an ever larger physical volume as the beam expands with distance: signals from more distant volumes suffer progressively increasing beam depolarization. The distance to the polarization horizon is beamwidth dependent, frequency dependent, and direction dependent. In the CGPS survey, with a $1'$ beam at 1420 MHz, the polarization horizon is at about 2 kpc between $\ell = 66^\circ$ and $\ell = 110^\circ$, so the polarization features detected arise within the Local arm. Beyond $\ell = 110^\circ$ the horizon moves into the Perseus arm, and towards the anticentre the telescope is seeing to the limit of the Galaxy (Landecker et al. 2010). Most of the imaging of the Galactic plane done to date has given us a very local view of the MIM. RM Synthesis can overcome some of the effects of Faraday thickness, but only high angular resolution can conquer beam depolarization.

RM Synthesis can offer information on distance, revealing the relative placement of RM features along the line of sight. It cannot give actual distances unless combined with other information and, possibly, combined with modelling.

4.3 Modelling and Statistical Approaches to Characterizing the Magneto-Ionic Medium

Modelling the total-intensity and polarized sky is a powerful technique for integrating many lines of astrophysical data.

On the basis of the 408 MHz all-sky map of Haslam et al. (1982), Beuermann et al. (1985) modelled the synchrotron emission from the Milky Way as a thin disk of scale height 150 pc within a thick disk whose scale height is 1.5 kpc (adapted to a distance to the Galactic centre of 8.5 kpc). The synchrotron scale height is produced by the combined effects of the scale heights of the magnetic field and of cosmic-ray electrons, and so the scale height of the magnetic field cannot be derived directly from the Beuermann et al. (1985) model. However, the scale height of the magneto-ionic disk may yield the desired information if coupled with measurements of the scale height of thermal electrons, recently estimated as 1.8 kpc (Gaensler et al. 2008). Measurements of the scale height of the RM disk of 1.4 kpc (Simard-Normandin and Kronberg 1980) are supported by recent measurements by Rae and Brown (2011), who find a value of 1.2 kpc in the outer Galaxy. Investigation of the roles of spiral structure and the Galactic warp is needed before the latter value can be translated to a scale height for the magnetic field. This is a developing subject.

The thorough work of Sun et al. (2008) is the first modelling effort to take radio polarization data into account, both RMs of extragalactic sources and data on diffuse emission. This is the most valuable contribution to understanding the magnetic field in the Galactic disk of recent years (see Sun and Reich (2010) for an improved estimate of the values of the halo field). The properties of the MIM, for which the evidence comes from radio polarization data, are crucial in the modelling. From this work, the large-scale field in the local vicinity has strength $\sim 2 \mu\text{G}$, and its configuration is well determined. The small-scale, random field strength is $\sim 3 \mu\text{G}$. The total field is lower than the equipartition value of $\sim 6 \mu\text{G}$ (Heiles 1995; Beck 2009), but the estimates are consistent within the errors. Strong depolarization evident between 23 GHz (Hinshaw et al. 2009) and 1.4 GHz (Wolleben et al. 2006) in a strip $-30^\circ < b < 30^\circ$ can be explained with a small filling factor of thermal electrons and a coupling of the random field with electron density (although an exact coupling factor could not be established).

The features visible in polarization images have often been described as “chaotic”, “disordered” or “patchy”. This structure is generally understood as the product of Faraday rotation in a turbulent magneto-ionic medium, and statistical analysis of its structure is a useful approach to uncovering the physics of the turbulence.

Observations of pulsar scintillation suggest that electron density variations on very small (sub-pc) scales exhibit Kolmogorov turbulence (Stinebring et al. 2000). On larger scales, Haverkorn et al. (2008) investigated structure functions of RMs of extragalactic sources. RM fluctuations are present in interarm regions up to scales of 100 pc, but in the arms there are no fluctuations beyond a few pc, much smaller than expected (values confirmed by estimates based on depolarization of extragalactic sources). These two very different values for the outer scales of the turbulence imply two different driving forces. Within the arms the dominant source of energy injection into turbulence is star-related activity (star formation, H II regions, stellar winds). Larger-scale effects appear to dominate in the interarm.

Sun and Reich (2009) have generated model radio images of total and polarized emission and RM at arcsecond resolution at various Galactic latitudes, based on their earlier modelling (Sun et al. 2008). These can provide the basis for comparison with observations via structure function or other techniques, and were created for use in simulations of the Square Kilometre Array.

“Canals” are long, thin features in polarization images where the polarized intensity drops to zero. Typically one beamwidth wide and many times as long, canals have apparently random locations and shapes. They were recognized first in A-S polarization images, but are also found in S-A data. The high-pass filtering of structure by A-S telescopes increases their number, but they nevertheless represent something real in the MIM. They have been variously interpreted as the boundaries between regions of different RM (Haverkorn et al. 2000, 2004), locations where differential Faraday rotation happens to lead to total depolarization (Shukurov and Berkhuisen 2003), or the locations of shock fronts (Haverkorn and Heitsch 2004; Fletcher and Shukurov 2006). Haverkorn and Heitsch (2004) used magnetohydrodynamic simulations of the turbulent ISM to show that shocks can generate RM gradients sufficiently steep to produce the observed effects.

While the small-scale field is quasi-random, Brown and Taylor (2001), examining RMs of extragalactic sources seen through the disk, found evidence of preferential alignment with the large-scale field. Their result applies to the outer Galaxy; such studies should be extended to other directions.

4.4 H II Regions

The effects of H II regions on polarization images have been discussed to some extent in Sect. 4.2. Intuitively one would expect that H II regions are depolarizers. Within them electron density is high and the ionized gas is generally turbulent, driven by winds and heating from the ionizing stars; field strengths should be high. The combination should result in strong Faraday rotation that changes quickly on small physical scales, leading to beam depolarization. Many observations confirm this view (Gray et al. 1999; Gaensler et al. 2001; Landecker et al. 2010), and it is further supported by the data of Stil and Taylor (2007) and Stil et al. (2011) who reported that some H II regions depolarize even compact extragalactic sources that are seen through them.

On the other hand there is recent evidence from the Urumqi survey at 4.8 GHz (Sun et al. 2007; Gao et al. 2010) that at least some H II regions act as Faraday screens but not as depolarizers. These authors report regions with electron densities a few electrons per cm^3 and fields up to $\sim 15 \mu\text{G}$, considerably stronger than the usual values of a few μG . It is not yet clear what mechanism can lead to these strong, well-organized fields. However, these regions seem to be closer to the regular Warm Ionized Medium than they are to classical H II regions, normally thought of as dense volumes ionized by one or more powerful stars.

If H II regions totally depolarize emission arising beyond them, then we can study synchrotron emissivity over local paths of known length on the near side (Uyaniker et al. 2003).

This is a new method that complements earlier results from absorption by H II regions at low frequencies (Roger et al. 1999; Nord et al. 2006) or from modelling (Beuermann et al. 1985; Sun et al. 2008).

Given the high sensitivity of radio telescopes to Faraday rotation, polarization data can be used to probe low-density envelopes of H II regions. Gray et al. (1999) examined the low-density ionized zone around W4. The W4 H II region is a strong depolarizer; at the edge of the depolarization zone the field strength is $\sim 20 \mu\text{G}$, and apparently scales as the square-root of electron density (but the data for this work do not include information on large structure, and the conclusions need to be revisited). These conditions rotate background emission but do not totally depolarize it.

Polarization observations can trace disk-halo interactions from H II complexes. The walls of the superbubble driven by the stars that excite W4 are detectable as depolarization features. West et al. (2007) estimated a magnetic field strength of 3 to $5 \mu\text{G}$ in the bubble walls based on an optical estimate of electron density ($\sim 0.4 \text{ cm}^{-3}$) and the observed degree of depolarization ($\sim 50\%$). Again, the data used in this work do not include large-scale structure. Duncan et al. (1997) observed depolarization “plumes” emanating from H II regions at $\ell = 288^\circ$ and $\ell = 292^\circ$ at latitudes just below $b = 0^\circ$, which they interpreted as vertical flows of ionized gas.

4.5 Photodissociation Regions

Wolleben and Reich (2004) observed Faraday rotation associated with the Taurus molecular cloud at 1400 and 1660 MHz (using the standard techniques of the EMLS). Information on large structure was available at 1400 MHz, and reasonable assumptions were used to derive such information at 1660 MHz. The data were fitted well with a model in which background emission is Faraday rotated in a thin “screen” of partially ionized material, a photodissociation region (PDR) on the surface of the molecular material, and adds vectorially to the foreground. Optical data place limits on electron density, making it possible to estimate field strength. The deduced magnetic field in the PDR is strong, $\sim 20 \mu\text{G}$, and it is well ordered. Local synchrotron emissivity deduced from the modeled foreground emission is quite high in relation to other estimates. The field estimate within this PDR has possibly been confirmed by H I Zeeman observations (Heiles and Robishaw 2009). Apparently similar PDR phenomena have been detected by Gao et al. (2010) on the edges of the W5 H II region.

4.6 Planetary Nebulae

Two planetary nebulae (PNe) have been identified as Faraday rotating objects in the CGPS survey (Table 1). The amounts of ionized material in these objects are small, of the order of $1 M_\odot$, yet, surprisingly, they generate unmistakable polarization signatures. Ransom et al. (2008) discuss Sh-2-216 ($\ell = 158.34^\circ$, $b = 0.2^\circ$)—see Fig. 1. Ransom et al. (2010) present data for DeHt 5 ($\ell = 111.1^\circ$, $b = 11.6^\circ$). Both objects appear as depolarization features: background polarized emission is Faraday rotated on passage through the ionized material and adds destructively to foreground emission.

Optical observations of Sh-2-216 yield good values of distance (allowing path length through the Faraday screen to be calculated) and electron density. The magnetic field can then be tightly constrained. The field in the shell is $\sim 5 \mu\text{G}$. This is probably interstellar field, slightly compressed, not stellar field (Ransom et al. 2008).

The progenitor of DeHt 5 has a high proper motion through the ISM. The PN itself is a depolarization feature. Ransom et al. (2010) also identify a series of patches of reduced

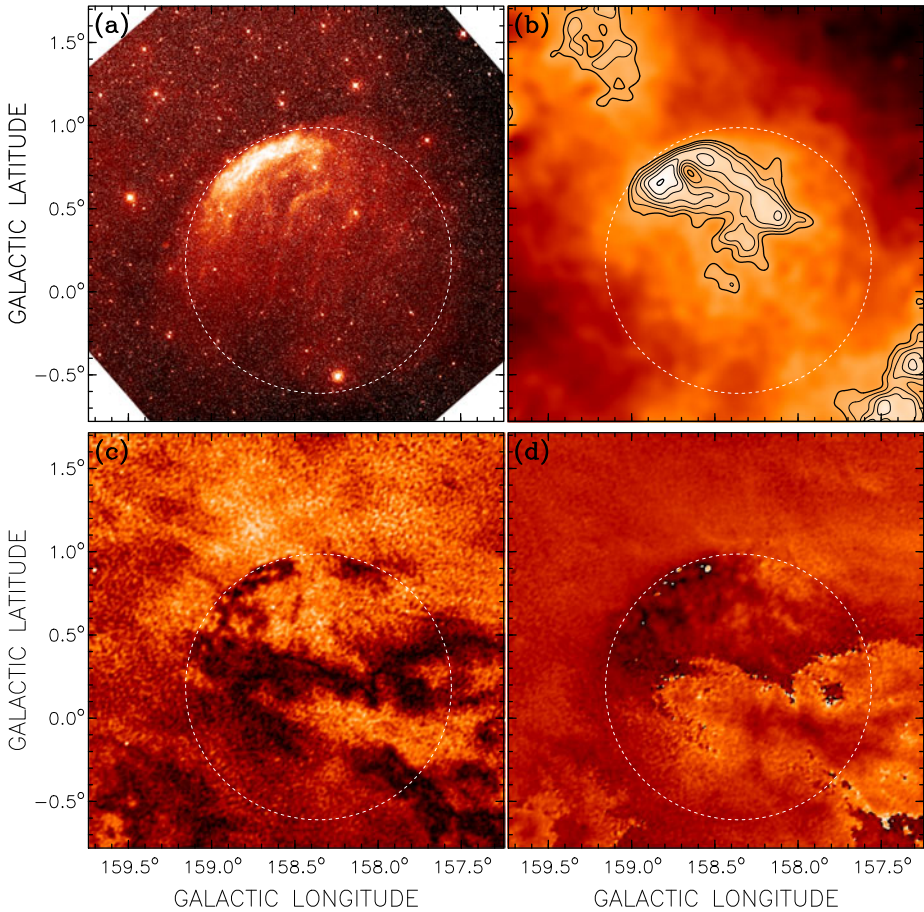


Fig. 1 The planetary nebula Sh 2-216 seen in optical emission (*top left*), total intensity at 1420 MHz (*top right*), polarized intensity (*bottom left*), and polarization angle (*bottom right*). The *dotted circle* outlines the optical emission. The central star has proper motion towards the bright optical rim in the north-east. An arc of depolarization corresponds to that rim. A superimposed feature confuses the polarized signal over the southern half of the object

polarized intensity *behind* this PN as relics of the winds from the progenitor during its AGB phase, prior to the formation of the PN. We are seeing a “magnetic wake” left behind as the star moves through the ISM. The wake consists of moving ionized material which drags field lines with it. The change in the line-of-sight component of the field generates the observed polarization signature.

There are several general conclusions. First, PNe could be used as probes of the Galactic magnetic field, as there is often useful optical data on distance, size, and electron density. High resolution aperture-synthesis telescopes (the VLA today, and especially the SKA in the future) could make similar observations of many PNe, reaching right across the Galaxy. Second, observations like these show that the (plentiful) low-mass stars contribute significant quantities of ionized material to the ISM.

4.7 Correlation of Polarization and H I Features

The new images of the Galactic ISM emerging from the CGPS, SGPS, and VGPS show that filamentary structure is a common feature of H I, in both cold and warm phases. The abundance of long, thin filaments is very suggestive that magnetic fields have played a role in forming or maintaining them. Only one observation bears on this question, the remarkable data of McClure-Griffiths et al. (2006). Long, thin filaments of cold gas, up to 17 pc long and less than 0.2 pc wide, were observed in self-absorption. The strands are aligned with the magnetic field direction deduced from polarization of starlight. The implied field strengths within the filaments, estimated using the Chandrasekhar and Fermi (1953) method, are $\geq 30 \mu\text{G}$ if the filaments are magnetically dominated (a field of this strength can hold the filaments straight against the effects of turbulence). Note that Heiles and Robishaw (2009) argue that the CF method overestimates the field. The features discussed by McClure-Griffiths et al. (2006) comprise cold gas. It is plausible that cold, dense filaments carry quite strong fields, since field is correlated with density (Sun et al. 2008), but that leaves open the question of the widespread filamentary features seen in emission from the (presumably) warm H I. Densities are lower and fields are probably lower too. No systematic search has been made for correlations between field and either cold or warm H I filaments; both starlight polarization data and radio polarization data will be useful.

5 Three Surveys that Overcome (Some of) the Limitations of Existing Data

In this section I describe three surveys that overcome some of the limitations that beset many of the efforts in Table 1.

5.1 Rotation Measure Synthesis with the Westerbork Telescope

Schnitzeler et al. (2007, 2009) have pioneered the use of RM Synthesis in the study of the extended Galactic emission. Using the Westerbork SRT with frequency coverage of 324 to 387 MHz yielded remarkably large coverage of the λ^2 domain, $0.6 \text{ m}^2 < \lambda^2 < 0.9 \text{ m}^2$, and excellent resolution in Faraday depth of 12 rad m^{-2} . They observed an area $7^\circ \times 7^\circ$ centred at $\ell \approx 181^\circ$, $b \approx 20^\circ$.

However, the absence of information at *short* wavelengths from these data imposed an upper limit to the largest Faraday depth that can be detected of $\sim 5 \text{ rad m}^{-2}$, smaller than the resolution in Faraday depth. This study therefore focused on a region with simple structure, the Galactic anticentre at high latitudes. Here the line of sight probes the Local arm and, possibly, the lower reaches of the Galactic halo. The regular component of the Galactic field is essentially perpendicular to the line of sight, producing relatively little Faraday rotation. These observations, then, have mostly probed the random field component. On the majority of the lines of sight RM spectra show only one peak, or two peaks with one dominant. The RM structure is indeed simple (at the resolution in Faraday space of these observations—increasing resolution will at some point encounter finer scales in the turbulence of the ISM).

Again exploiting the simplicity of the anticentre Schnitzeler et al. (2009) used WHAM H α data (Haffner et al. 2003) to provide values of emission measure. Translating those to dispersion measure led to values of the line-of-sight component of the magnetic field. The angular resolution is limited by the 1° beam of the WHAM data, but coverage of the field is complete since there is little optical extinction. The deduced field values ($0 < \langle B_{\parallel} \rangle < 0.75 \mu\text{G}$) are larger than the anticipated value of the regular field (nearly zero

in this direction), but substantially smaller than the $3 \mu\text{G}$ random component estimated by Sun et al. (2008), possibly because of the 1° effective resolution.

Extragalactic sources seen in this region show RM values comparable to the Faraday depths of the extended emission, indicating that the emitting and Faraday rotating regions are entirely within the polarization horizon (Sect. 4.2). This is not the case in more complex directions (towards the inner Galaxy), indicating again the simplicity of these lines of sight in the anticentre. However, this comparison is possible over only half the area. In the other half the number of polarized background sources detected was insufficient for any definite conclusion. It is instructive that measurements of the extended Galactic emission can give almost complete sampling of Faraday depth while simultaneous observations of extragalactic sources with the same telescope can give only sparse data.

5.2 The CGPS Polarization Survey

The Canadian Galactic Plane Survey (Taylor et al. 2003, the CGPS) set out to observe the major constituents of the ISM with arcminute resolution.¹ As part of the CGPS, the polarized emission at 1420 MHz along the northern Galactic plane has been imaged using the DRAO Synthesis Telescope (Landecker et al. 2010). Observations at 1420 MHz in Stokes parameters I , Q , and U cover $\ell = 66^\circ$ to $\ell = 175^\circ$ over a range $-3^\circ < b < 5^\circ$, with an extension from $\ell = 101^\circ$ to $\ell = 116^\circ$ up to $b = 17.5^\circ$. Angular resolution is $\sim 1'$. The survey brings together data from three telescopes. The DRAO Synthesis Telescope (Landecker et al. 2000) provided arcminute resolution, and the images were accurately corrected for instrumental polarization across the field of view (Reid et al. 2008). Structures larger in size than about $20'$, undersampled or missing in the A-S data, were incorporated from the Effelsberg Medium-Latitude Survey—the EMLS—(Reich et al. 2004) and structures larger than $\sim 5^\circ$, missing from the EMLS data because of the observing and processing techniques used (Sect. 3.2), were derived from the survey made with the DRAO 26-m Telescope (Wolleben et al. 2006). Evaluation of the relative scales of three sets of observations with quite distinct telescopes has an accuracy of about $\pm 10\%$, set by the accuracy of knowledge of the S-A beamshapes (Landecker et al. 2010). This is the first extensive survey of the Galactic polarized emission to incorporate S-A with A-S data, and, covering 1060 square degrees with 1.5×10^7 independent data points, is the largest polarization survey ever.

5.3 Results from the CGPS Polarization Survey

Some of the polarized features found in the CGPS polarization survey are discussed in Landecker et al. (2010); in this section I discuss only one. Figure 2 shows a polarized intensity (PI) image from the CGPS together with an H I image at $v_{LSR} = -20 \text{ km s}^{-1}$. There is a very clear association of the polarized arc that starts at $\ell = 162^\circ$, $b = 2.4^\circ$, and curves across the top of the PI image, with an H I feature. Total extent of these features is $162^\circ \leq \ell \leq 170^\circ$, 8° in longitude.

The association with H I immediately provides a kinematic distance, approximately 1.9 kpc, which places this object in the Perseus arm and implies a linear extent of about 350 pc. The interpretation (Kothés et al. in preparation) sees this as a large stellar-wind bubble (SWB), the product of a cluster of massive stars. In the SWB model of Weaver et al.

¹The Canadian Galactic Plane Survey database is accessible to the worldwide astronomy community at <http://www3.cadc-ccda.hia-ihp.nrc-cnrc.gc.ca/cgps/>.

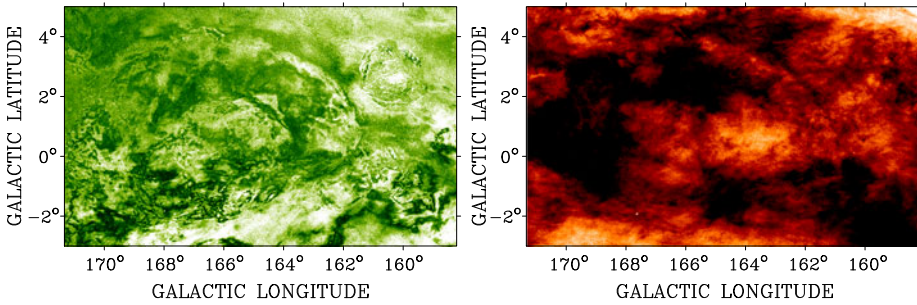


Fig. 2 CGPS data, 1420 MHz, angular resolution $1'$. Polarized intensity (*left*) from 0 (*black*) through *green* to 500 mK (*white*), and H I at $v_{LSR} = -20 \text{ km s}^{-1}$ from 20 (*white*) through *red* to 80 K (*black*)

(1977) there is a central hot-wind region where the temperature, T , is 10^6 K and the electron density, n_e , is 0.01 cm^{-3} , surrounded by a shocked-wind region where $T = 10^5 \text{ K}$ and n_e is higher (in this paragraph all numbers should be read as approximate). A very simple Faraday rotation model with a toroidal magnetic field of strength $30 \mu\text{G}$ in the shocked wind zone and $n_e = 0.2 \text{ cm}^{-3}$ can explain the PI and polarization angle manifestations of this object. Synchrotron emission from a smooth background is Faraday rotated in the shocked-wind zone, and vector addition with polarized foreground emission produces increases and decreases in PI that define the structure seen in the figure.

Once detected, other manifestations of the SWB became evident: X-rays from hot gas in the interior: evidence of the expansion of the H I shell from absorption spectra of background compact sources seen through it: a clear association with the supernova remnant G166.0+4.3. The SWB has an age of $1\text{--}2 \times 10^7$ years, but all surrounding objects are younger, $\sim 1 \times 10^6$ years, and there is evidence that the large SWB has triggered star formation in its environs.

This result has several implications. First, the strong toroidal magnetic field evident in this SWB is probably generated by winding up a radial field arising from stellar winds. The field may have been enhanced by magnetized material carried out from massive stars by the winds. Compression by the expansion may have amplified the field further. Second, this is an example of a large and significant object that remained hidden until detected by its Faraday rotation, and a powerful demonstration of the sensitivity of polarization observations as detectors of ionized gas. Third, modelling of the region would be meaningless, and so interpretation would be very difficult, if data on broad structure were not incorporated in the images (the object can be seen in the EMLS data (Reich et al. 2004) but interpretation could not proceed from those data alone). Fifth, arcminute resolution was instrumental in the recognition of the SWB, and helped refine model parameters. Sixth, most significantly, observations of this object would be very difficult to understand without complementary data on other ISM tracers.

5.4 The Global Magneto-Ionic Medium Survey

The Global Magneto-Ionic Medium Survey—GMIMS—(Wolleben et al. 2009) sets out to map the polarized emission from the entire sky, North and South, using large single antennas over the entire frequency range 300 to 1800 MHz. It brings together three technologies, (a) wideband feeds for reflector antennas, (b) FPGA-based spectropolarimeters with several thousand frequency channels, and (c) RM Synthesis. The survey task has been divided

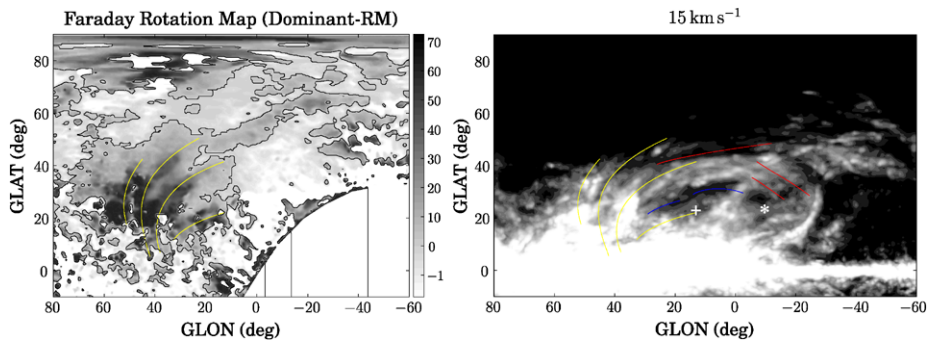


Fig. 3 The *left image* shows Faraday depth in a $90^\circ \times 140^\circ$ region with angular resolution 1° . For each pixel the position in rad m^{-2} of the strongest peak in the RM-Synthesis spectrum is shown, with black indicating the most positive values. Superimposed *yellow curves* trace four “filaments” of strong positive RM. The *right image* of the same area shows HI at $v_{LSR} = 15 \text{ km s}^{-1}$ from the LAB Survey. The filaments from the *left panel* are reproduced (*yellow*), and *red lines* trace filaments detected at negative values of RM

Table 2 Surveys of the Galactic polarized emission underway but not published

Survey	Ref.	ν [MHz]	θ [']	A-S	S-A	Large Scale	RM Synth.
GALFACTS	(1)	1225–1525	3		y	y	y
GMIMS-HBN	(2)	1277–1762	40–30		y	y	y
GMIMS-HBS	(3)	1300–1800	10		y	y	y
GMIMS-LBS	(3)	300–470 & 660–870	60–20		y	y	y
SPASS	(4)	2300	8.9		y	y	y
CBASS	(5)	5000	44		y	y	

References: (1) Taylor and Salter (2011), (2) Wolleben et al. (2010a), (3) Wolleben et al. (2009), (4) Carretti (2011), (5) King et al. (2010)

Notes: (a) Headings and abbreviations are as in Table 1. (b) GMIMS surveys are labeled HBN (High-Band North), HBS (High-Band South), and LBS (Low-Band South). Mid-Band surveys, covering ~ 800 to ~ 1300 MHz, have not been started yet

between the Northern and Southern hemispheres and the frequency band has been divided into three sub-bands, dictated by receiver technology (see Table 2). The survey technique of Carretti (2011) will be used wherever possible, and intensity scales will be absolutely calibrated.

5.5 Results from the Global Magneto-Ionic Medium Survey

GMIMS High-Band North using the DRAO Telescope (Wolleben et al. 2010a) represents the first use of RM Synthesis with a single-antenna telescope. The value of such data, even at an angular resolution of $\sim 1^\circ$, is revealed by the data shown in Fig. 3 (reproduced from Wolleben et al. 2010b). Once again, complementary data on other ISM constituents have been an indispensable aid to interpretation.

The left panel shows a map of Faraday depth derived from RM Synthesis of the data cube. At each pixel of the image, the Faraday depth of the strongest polarized emission is plotted.

Filaments are identifiable in this image (traced by lines superimposed on the grayscale). These convincingly coincide with one side of an H I bubble, 100×200 pc in size, seen in the LAB Survey (Kalberla et al. 2005). The boundary of the H I bubble at $\ell \approx 40^\circ$ coincides with emission with positive RM, while the boundary near $\ell \approx -25^\circ$ coincides with negative RM. This suggests a magnetic field wrapped around the bubble. The implied field strength in the shell is between 20 and 34 μG . The H I bubble may be expanding within the dense wall of the local bubble, the strong field arising from further compression of an already compressed plasma.

6 Concluding Discussion

The observations reviewed have provided opportunities to measure line-of-sight magnetic fields in a variety of ISM situations. The field values, sometimes as high as 30 μG , are well above the local value of ~ 2 μG , presumably as a result of compression. As evidence like this accumulates it will inform theory-based models of the ISM. An example is provided by the work of de Avillez and Breitschwerdt (2005). Using MHD code, they have run a massive computation tracking the evolution of the magnetized ISM, driven by star formation, stellar winds, supernovae, etc. After 3.5×10^8 years the total field averages to 4.4 μG , it is concentrated in the walls of bubbles and superbubbles whose expansion is controlled by it, but field strength remains uncorrelated with density. The filling factor of hot ($\geq 10^{5.5}$ K) gas is $\sim 20\%$. We are on the verge of having polarization data useful for comparison with all-encompassing models like this.

The magnetic field should not be considered alone, but as a constituent of the ISM. Polarization data will always be easier to understand when seen in the context of observations of other constituents of that complex system.

7 The Future

Advances in understanding the interplay of magnetic fields and the ISM will come from observations with high angular resolution, full coverage of all spatial scales, and excellent resolution in Faraday depth. These requirements will be met by combining A-S and S-A data.

Table 2 lists polarization surveys being carried out with existing telescopes, and surveys approved and funded. All employ single-antenna telescopes. The GMIMS surveys will provide excellent frequency coverage and, consequently, very good resolution in Faraday depth, but only with the angular resolution available with S-A telescopes. The only survey whose angular resolution approaches the desired one arcminute is GALFACTS.

Beyond that lies the prospect of the new aperture-synthesis telescopes, LOFAR (already operating), ASKAP, and MeerKAT. All are designed as survey telescopes. All have high angular resolution, and all will produce wideband multi-channel data amenable to RM synthesis. The POSSUM survey (Gaensler et al. 2010), using the ASKAP telescope, will provide spectropolarimetric data at least from 1130 to 1430 MHz. All surveys with these A-S telescopes will require combination with single-antenna data (with the possible exception of LOFAR at the low end of its frequency range). Interpretation of the wealth of new data will benefit from the approach promoted here, one that views the magnetic field as a constituent of the ISM, and interprets polarization observations in conjunction with data on other ISM tracers. I have made many suggestions in Sect. 4 of topics where further investigation could be profitable, and I fully expect that the new instruments will lead to rapid progress along such paths in understanding the role that magnetic fields play in the Galactic ecosystem.

References

- R. Beck, *Space Sci. Rev.* **99**, 243 (2001)
- R. Beck, *Astrophys. Space Sci. Trans.* **5**, 43 (2009)
- G. Bernardi, A.G. de Bruyn, M.A. Brentjens et al., *Astron. Astrophys.* **500**, 965 (2009)
- K. Beuermann, G. Kanbach, E.M. Berkhuijsen, *Astron. Astrophys.* **153**, 17 (1985)
- M.A. Brentjens, A.G. de Bruyn, *Astron. Astrophys.* **441**, 1217 (2005)
- W.N. Brouw, T.A.T. Spoelstra, *Astron. Astrophys. Suppl.* **26**, 129 (1976)
- J.C. Brown, in *ASP Conference Series*, vol. 438 (2011) p. 216
- J.C. Brown, A.R. Taylor, *Astrophys. J. Lett.* **563**, 31 (2001)
- J.C. Brown, A.R. Taylor, B.J. Jackel, *Astrophys. J. Suppl.* **145**, 213 (2003)
- J.C. Brown, M. Haverkorn, B.M. Gaensler et al., *Astrophys. J.* **663**, 258 (2007)
- B.J. Burn, *Mon. Not. R. Astron. Soc. Lett.* **133**, 67 (1966)
- E. Carretti, in *ASP Conference Series*, vol. 438 (2011), p. 277
- E. Carretti, M. Haverkorn, D. McConnell et al., *Mon. Not. R. Astron. Soc. Lett.* **405**, 1670 (2010)
- S. Chandrasekhar, E. Fermi, *Astrophys. J.* **118**, 116 (1953)
- D.P. Clemens, A. Pinnick, M. Pavel et al., in *Bulletin of the American Astronomical Society*, vol. 43 (2011), 241-15
- M.A. de Avillez, D. Breitschwerdt, *Astron. Astrophys.* **436**, 585 (2005)
- J.M. Dickey, *Astrophys. J.* **488**, 258 (1997)
- A.R. Duncan, R.F. Haynes, K.L. Jones, R.T. Stewart, *Mon. Not. R. Astron. Soc. Lett.* **291**, 279 (1997)
- A.R. Duncan, P. Reich, W. Reich, E. Fürst, *Astron. Astrophys.* **350**, 447 (1999)
- A. Fletcher, A. Shukurov, *Mon. Not. R. Astron. Soc. Lett.* **371**, 25 (2006)
- P. Fosalba, A. Lazarian, S. Prunet, J.A. Tauber, *Astrophys. J.* **564**, 762 (2002)
- P. Frick, D. Sokoloff, R. Stepanov, R. Beck, *Mon. Not. R. Astron. Soc. Lett.* **401**, 24 (2010)
- P. Frick, D. Sokoloff, R. Stepanov, R. Beck, *Mon. Not. Roy. Astron. Soc.*, 557 (2011)
- B.M. Gaensler, J.M. Dickey, N.M. McClure-Griffiths et al., *Astrophys. J.* **549**, 959 (2001)
- B.M. Gaensler, G.J. Madsen, S. Chatterjee, S.A. Mao, *Publ. Astron. Soc. Aust.* **25**, 184 (2008)
- B.M. Gaensler, T.L. Landecker, A.R. Taylor, POSSUM Collaboration, in *Bulletin of the American Astronomical Society*, vol. 41 (2010), p. 515
- X.Y. Gao, W. Reich, J.L. Han et al., *Astron. Astrophys.* **515**, 64 (2010)
- A.D. Gray, T.L. Landecker, P.E. Dewdney et al., *Astrophys. J.* **514**, 221 (1999)
- L.M. Haffner, R.J. Reynolds, S.L. Tufte et al., *Astrophys. J. Suppl.* **149**, 405 (2003)
- J.L. Han, in *IAU Symposium*, vol. 259 (2009), p. 455
- J.L. Han, R.N. Manchester, E.M. Berkhuijsen et al., *Astron. Astrophys.* **322**, 98 (1997)
- C.G.T. Haslam, C.J. Salter, H. Stoffel, W.E. Wilson, *Astron. Astrophys. Suppl.* **47**, 1 (1982)
- M. Haverkorn, F. Heitsch, *Astron. Astrophys.* **421**, 1011 (2004)
- M. Haverkorn, P. Katfert, A.G. de Bruyn, *Astron. Astrophys.* **356**, 13 (2000)
- M. Haverkorn, P. Katfert, A.G. de Bruyn, *Astron. Astrophys.* **403**, 1031 (2003)
- M. Haverkorn, P. Katfert, A.G. de Bruyn, *Astron. Astrophys.* **427**, 549 (2004)
- M. Haverkorn, B.M. Gaensler, N.M. McClure-Griffiths et al., *Astrophys. J. Suppl.* **167**, 230 (2006)
- M. Haverkorn, J.C. Brown, B.M. Gaensler, N.M. McClure-Griffiths, *Astrophys. J.* **680**, 362 (2008)
- G. Heald, in *IAU Symposium*, vol. 259 (2009), p. 591
- C. Heiles in *ASP Conference Series*, vol. 80 (1995), p. 507
- C. Heiles, T. Robishaw, in *IAU Symposium*, vol. 259 (2009), p. 579
- G. Hinshaw, J.L. Weiland, R.S. Hill et al., *Astrophys. J. Suppl.* **180**, 225 (2009)
- N. Junkes, E. Fürst, W. Reich, *Astron. Astrophys. Suppl.* **69**, 451 (1987)
- P.M.W. Kalberla, W.B. Burton, D. Hartmann et al., *Astron. Astrophys.* **440**, 775 (2005)
- O.G. King, C. Copley, R. Davies et al., in *Society of Photo-Optical Instrumentation Engineers (SPIE) Conference Series*, vol. 7741 (2010)
- R. Kothes, T.L. Landecker, M. Wolleben, *Astrophys. J.* **607**, 855 (2004)
- T.L. Landecker, P.E. Dewdney, T.A. Burgess et al., *Astron. Astrophys. Suppl.* **145**, 509 (2000)
- T.L. Landecker, W. Reich, R.I. Reid et al., *Astron. Astrophys.* **520**, 80 (2010)
- N.M. McClure-Griffiths, A.J. Green, J.M. Dickey et al., *Astrophys. J.* **551**, 394 (2001)
- N.M. McClure-Griffiths, J.M. Dickey, B.M. Gaensler et al., *Astrophys. J.* **652**, 1339 (2006)
- M.E. Nord, P.A. Henning, R.J. Rand et al., *Astron. J.* **132**, 242 (2006)
- A. Noutsos, *Space Sci. Rev.* (2011, this issue)
- K.M. Rae, J.C. Brown, in *ASP Conference Series*, vol. 438 (2011), p. 229
- R.R. Ransom, B. Uyaniker, R. Kothes, T.L. Landecker, *Astrophys. J.* **684**, 1009 (2008)
- R.R. Ransom, R. Kothes, M. Wolleben, T.L. Landecker, *Astrophys. J.* **724**, 946 (2010)
- W. Reich, in *Cosmic Polarization*, ed. by R. Fabbri (2006), p. 91

- W. Reich, E. Fürst, P. Reich et al., in *The Magnetized Interstellar Medium, Antalya, Turkey*, ed. by B. Uyaniker, W. Reich, R. Wielebinski (2004), p. 45
- R.I. Reid, A.D. Gray, T.L. Landecker, A.G. Willis, *Radio Sci.* **43**, 2008 (2008)
- R.S. Roger, C.H. Costain, T.L. Landecker, C.M. Swerdlyk, *Astron. Astrophys. Suppl.* **137**, 7 (1999)
- L. Rudnick, S. Brown, *Astron. J.* **137**, 145 (2009)
- D.H.F.M. Schnitzeler, P. Katgert, A.G. de Bruyn, *Astron. Astrophys.* **471**, 21 (2007)
- D.H.F.M. Schnitzeler, P. Katgert, A.G. de Bruyn, *Astron. Astrophys.* **494**, 611 (2009)
- D.H.F.M. Schnitzeler, P. Katgert, M. Haverkorn, A.G. de Bruyn, *Astron. Astrophys.* **461**, 963 (2007)
- A. Shukurov, E.M. Berkhuijsen, *Mon. Not. R. Astron. Soc. Lett.* **342**, 496 (2003)
- M. Simard-Normandin, P.P. Kronberg, *Astrophys. J.* **242**, 74 (1980)
- D.D. Sokoloff, A.A. Bykov, A. Shukurov, E.M. Berkhuijsen, R. Beck, A.D. Poezd, *Mon. Not. R. Astron. Soc. Lett.* **299**, 189 (1998)
- T.A.T. Spoelstra, *Astron. Astrophys.* **135**, 238 (1984)
- J.M. Stil, A.R. Taylor, *Astrophys. J. Lett.* **663**, 21 (2007)
- J.M. Stil, A.R. Taylor, C. Sunstrum, *Astrophys. J.* **726**, 4 (2011)
- J.M. Stil, A.R. Taylor, J.M. Dickey et al., *Astron. J.* **132**, 1158 (2006)
- D.R. Stinebring, T.V. Smirnova, T.H. Hankins et al., *Astrophys. J.* **539**, 300 (2000)
- X.-H. Sun, W. Reich, *Astron. Astrophys.* **507**, 1087 (2009)
- X.-H. Sun, W. Reich, *Res. Astron. Astrophys.* **10**, 1287 (2010)
- X.H. Sun, J.L. Han, W. Reich et al., *Astron. Astrophys.* **469**, 1003 (2007)
- X.H. Sun, W. Reich, A. Waelkens, T.A. EnBlin, *Astron. Astrophys.* **477**, 573 (2008)
- A.R. Taylor, S.J. Gibson, M. Peracaula et al., *Astron. J.* **125**, 3145 (2003)
- A.R. Taylor, C.J. Salter in *ASP Conference Series*, vol. 438 (2011), p. 402
- J.C. Testori, P. Reich, W. Reich, *Astron. Astrophys.* **484**, 733 (2008)
- B. Uyaniker, T.L. Landecker, A.D. Gray, R. Kothes, *Astrophys. J.* **585**, 785 (2003)
- C.L. Van Eck, J.C. Brown, J.M. Stil et al., *Astrophys. J.* **728**, 97 (2011)
- R. Weaver, R. McCray, J. Castor et al., *Astrophys. J.* **218**, 377 (1977)
- J.L. West, J. English, M. Normandeau, T.L. Landecker, *Astrophys. J.* **656**, 914 (2007)
- G. Westerhout, C.L. Seeger, W.N. Brouw, J. Tinbergen, *Bull. Astron. Inst. Neth.* **16**, 187 (1962)
- R. Wielebinski, J.R. Shakeshaft, I.I.K. Pauliny-Toth, *The Observatory* **82**, 158 (1962)
- A. Wilkinson, *Mon. Not. R. Astron. Soc. Lett.* **163**, 147 (1973)
- M. Wolleben, W. Reich, *Astron. Astrophys.* **427**, 537 (2004)
- M. Wolleben, T.L. Landecker, W. Reich, R. Wielebinski, *Astron. Astrophys.* **448**, 411 (2006)
- M. Wolleben, T.L. Landecker, E. Carretti et al., in *IAU Symposium* vol. 259 (2009), p. 89
- M. Wolleben, T.L. Landecker, G.J. Hovey et al., *Astron. J.* **139**, 1681 (2010a)
- M. Wolleben, A. Fletcher, T.L. Landecker et al., *Astrophys. J. Lett.* **724**, 48 (2010b)